Remote Sensing of Environment 231 (2019) 111226

Contents lists available at ScienceDirect

Remote Sensing of Environment

journal homepage: www.elsevier.com/locate/rse

Quantification of irrigation water using remote sensing of soil moisture in a semi-arid region

Ehsan Jalilvand[a,*], Masoud Tajrishy[a], Sedigheh Alsadat Ghazi Zadeh Hashemi[a], Luca Brocca[b]

[a] Department of Civil and Environmental Engineering, Sharif University of Technology, Tehran, Iran
[b] Research Institute for Geo-Hydrological Protection, National Research Council, Perugia, Italy

ARTICLE INFO

Keywords:
Irrigation
Soil moisture
Remote sensing
SM2RAIN
AMSR2
Semi-arid region

ABSTRACT

Irrigated agriculture is the principal consumer of fresh water resources. Most countries do not have a precise measurement of water consumption for irrigation. In this study, an innovative approach is proposed that allows for estimation of irrigation water use at the catchment scale based on satellite soil moisture data. To this end, the SM2RAIN algorithm, which had been originally developed for estimation of rainfall from the soil moisture observations, is adopted. The satellite soil moisture observations obtained from Advanced Microwave Scanning Radiometer 2 (AMSR2) along with different rainfall and evapotranspiration (ET) products in the period 2012–2015 are used as the input to the model. The methodology is tested in the agricultural plains of southern Urmia Lake, which is one of the main agricultural plains in Iran for which actual irrigation data is available.

The results reveal that the proposed approach can capture the overall irrigation pattern, although; it is systematically overestimating irrigation volume compared to observed irrigation data. Thus the bias is calculated over largely non-irrigated pixels and used to modify the model estimates. The bias-corrected results show good agreement with the in situ irrigation data. In particular, the average model performance in the irrigated pixels in terms of R and RMSE (mm/month) are (0.86 and 12.895) respectively. Accuracy varied depending on the inputs, with improvement in order of 11% and 42% in R and RMSE depending on the inputs chosen. The method is also applied to less irrigated areas that result in obtaining significantly lower irrigation rates.

The low spatial resolution of soil moisture products (i.e. ~50 km) makes it difficult to capture the irrigation water of small irrigated croplands. Unreliable rainfall and ET data can also lead to the over/underestimation of irrigation. In spite of the above limitations (particularly lack of reliable ET dataset), the proposed model can still capture the irrigation pattern, given that strong soil moisture signal from irrigation is detected by the satellite.

1. Introduction

Seventy percent of water withdrawn from lakes, rivers, and ground water aquifers is used for irrigation. Irrigated agriculture is the principal consumer of fresh water resources worldwide (Thomson, 2003). As the earth's population increase in future, the demand for food will increase. To supply this growing demand, the entire world, and especially arid and semi-arid regions, will require a significant expansion and intensification of the irrigation agriculture (Ozdogan et al., 2010). In this regard improving the irrigation measurement techniques can have a great impact on the efficiency and management of irrigation at large scale. Moreover, estimating irrigation water can contribute to assessing irrigation water food production (Vörösmarty et al., 2000), modelling irrigation water requirements at the global scale (Döll and Siebert, 2002) and quantifying the impact of irrigation on hydrometric variables such as river discharge (Alter et al., 2015; Haddeland et al., 2007) and ground water (Breña-Naranjo et al., 2014).

The studies employing remote sensing observations for irrigation estimation are usually following three main objectives: (1) detection of the irrigation signal or irrigation mapping; (2) quantifying the irrigation amount; and (3) detecting the seasonal timing of irrigation. A number of key studies that address these objectives are summarized in Table 1.

Remote sensing has been an effective tool to monitor irrigated lands in many locations around the world as their spectral responses are different from non-irrigated croplands (Ozdogan et al., 2010). This has been accomplished using optical sensors including Landsat, MODIS (Moderate Resolution Imaging Spectroradiometer), AVHRR (Advanced Very High Resolution Radiometer) and SPOT (Satellite pour 1′Observation de la Terre) (Ozdogan et al., 2010; Peña-Arancibia et al.,

* Corresponding author.
E-mail address: ehsan.jalilvand@sharif.edu (E. Jalilvand).

https://doi.org/10.1016/j.rse.2019.111226
Received 20 August 2018; Received in revised form 22 May 2019; Accepted 28 May 2019

Table 1
Summary of relevant literature on the irrigation detection and quantification using satellite data (the current paper is added for completeness) with three main goals: (1) detection of the irrigation signal or irrigation mapping; (2) quantifying the irrigation amount; and (3) detecting the seasonal timing of irrigation that is shown in the key results column. Goals that are not addressed in a paper are denoted with N/A, i.e., 'not applicable'.

no	Technique	data	Resolution	Method	Key results	Reference
1	Optical	2001	500 m	Irrigation mapping using classification-based procedure that utilizes MODIS time series data coupled with ancillary data on climate and agricultural extent (case study: Continental US)	(1) Irrigated cropland is detected with higher accuracy under dryland irrigation condition (2) N/A (3) N/A	Ozdogan and Gutman (2008)
2		2005–2012	30 m	Mapping summer crop irrigation using Random Forrest classification method and a combination of remotely sensed vegetation phenology and water use data, such as Actual Evapotranspiration (ETa), as the inputs, (case study: Murray–Darling Basin in Australia)	(1) The most important predictors for mapping the irrigated area are remotely sensed vegetation phenology and ETa surplus over Precipitation (2) N/A (3) N/A	Peña-Arancibia et al. (2014)
3		2000–2015	250 m 56 m	Using seasonal peaks of NDVI in a hierarchal decision model to develop annual irrigation binary map (case study: India)	(1) Irrigated Area is mapped with high accuracy (R^2 = 0.95). Dramatic decline in irrigated area are observed in drought years. (2) N/A (3) N/A	Ambika et al. (2016)
4	Optical/Land Surface Model (LSM)	2001–2010 (China) 2010–2012 (Africa)	30 km 3 km	Calculating the difference in actual ET estimated by a remote sensing method that consider irrigation and a LSM (GLDAS) that does not incorporate irrigation to monitor irrigation practices	(1) Detecting irrigated croplands (2) Estimating the value and source of irrigation (3) Detecting seasonal and inter -annual trends	Romaguera et al. (2014)
5		2000–2012	4 km	Mapping nan-precipitation sink/source process (including irrigation) by comparing latent heat flux estimates by ALEXI and NOAH LSM (case study: CONUS)	(1) Good matches between the model outputs and known spatial variations of groundwater depth and irrigation extent were obtained. (2) N/A (3) N/A	Hain et al. (2015)
6	Microwave (MW)/ LSM	2000 2012, 2013	~25–50 km	Subtracting Satellite SM from Model SM assuming model doesn't incorporate irrigation	(1) Most satellite SM products are not skillful enough to detect irrigated areas over CONUS, some potential is observed using ASCAT in Nebraska (2) N/A (3) N/A	Kumar et al. (2015)
7		2010–2011	25 km 5 km	Subtracting Satellite SM from Model SM data assuming model doesn't incorporate irrigation (case study: The Northeast of the Iberian Peninsula)	(1) SMOS is the only SM product (compare to ASCAT and AMSR2) that was able to detect irrigation (2) N/A (3) N/A	Escorihuela and Quintana-Seguí (2016)
8	MW/Optical	2002–2011	25 km 1 km	Using AMSR-E SM alongside the SPOT NDVI data for observing the dynamic pattern of irrigation/agricultural practice over north western of India	(1) N/A (2) N/A (3) It was able to detect the shift in irrigation practices	Singh et al. (2017)
9	MW	1996–2010	25 km	Assessing spatial and the observed trend consistency between satellite SM, model SM and in situ precipitation data over irrigated croplands in China	(1) N/A (2) N/A (3) discrepancy between satellite SM and in situ precipitation is observed over major irrigation regions of China	Qiu et al. (2016)
10		2016	9 km	Comparing satellite SM data and precipitation data over 3 major irrigation area in US	(1) Able to find irrigation spatial signature using SMAP enhanced 9 km SM product (2) N/A (3) Detecting seasonal timing of irrigation	Lawston et al. (2017)
11		2012–2015	25 km	Applying SM2RAIN algorithm for estimating irrigation over irrigated croplands in NW of Iran (semi-arid region) using satellite soil moisture data	(1) N/A (2) The estimated irrigation amount is compatible with in situ irrigation data (3) The model capture the seasonal timing of the irrigation corresponding with in situ data	This study

2014). For instance, Ozdogan and Gutman, 2008 compared different maps of irrigated areas across the continental US that were produced using different satellite sensors and methodologies, which highlighted substantial agreement among these maps. Ambika et al. (2016) developed a multi-year (2000–2015) dataset of high-resolution irrigated area maps from MODIS NDVI and land use/land cover data with satisfactory accuracy. Peña-Arancibia et al. (2014) applied random forrest classification technique to a combination of remotly sense vegatation and water use indices (such as ETa and its surplus over precipitation) to map irrigated cropland during the summer in the Murray–Darling Basin in Australia. The results indicate that incorporating water use indices enhanced the model capability in depiction of the irrigation croplands. Similarly, several examples of irrigated area maps obtained from optical and visible sensors have been produced to date (Ozdogan et al., 2010).

In recent years, satellite soil moisture products have also been introduced as a tool for detecting irrigated areas. The first study in this regard was carried by (Kumar et al., 2015) who used satellite soil moisture observations from ASCAT (Advanced SCATterometer), AMSR-E (Advanced Microwave Scanning Radiometer - Earth Observing System), SMOS (Soil Moisture and Ocean Salinity), ESA CCI SM (Europan Space Agency Climate Change Initiative Soil Moisture) and Windsat, together with modelled data from Noah land surface model (LSM), to detect irrigation over the continental US. In this approach a comparison was made between the cumulative density function of a modelled soil moisture data (not incorporating irrigation) and corresponding satellite measurements. Where satellite product shows wetter soil moisture condition (compared to modelled data) irrigation was inferred. While the use of ASCAT soil moisture product showed promising results in detection of irrigation in specific areas (the plain of Nebraska), the spatial mismatch between model and observation data and confounding effects of topography, vegetation, frozen soils and RFI (Radio Frequency Interference) prevented a clear identification of irrigated areas in most regions. A similar approach has been used in many other studies, for instance, Escorihuela and Quintana-Seguí (2016) compared satellite soil moisture (ASCAT, AMSR-E, SMOS and SMOScat – a MODIS-downscaled version of SMOS product) and modelled data (by SURFEX - Surface Externalisée - land surface model) in the North-east of the Iberian Peninsula. For the high resolution SMOScat product (1 km), a clear decrease in correlation between modelled and satellite data was observed for a small heavily irrigated region. Again, the land surface model does not account for irrigation, thus the low correlation was an indication of irrigation practices. SMOScat is also used in another study by Malbéteau et al., 2018, in which SM data is assimilated into a simple force-restore soil hydric budget model. As this model is only forced by rainfall, timing of irrigation was detected where significant difference exist between the SMOScat SM and the offline prediction with the soil model.

Beside SM, other water balance components are also employed to map irrigation using the abovementioned approach. For instance, in a study by Hain et al., 2015 over Contiguous United States (CONUS), the estimated ET by Noah LSM,v 3.2 (not incorporating non-precipitation water sources) was compared against remotely sensed ETa product (ALEXI-the Atmosphere-Land Exchange Inverse model) which is an energy balance approach that take into account all the fluxes (including irrigation) that alter the surface energy balance. The excess ET estimated by ALEXI was attributed to the irrigation. While large scale irrigation agriculture could be mapped by this approach, shortcomings such as overestimation of ET in train-shading by ALEXI, the inherent error in Noah LSM estimates and several other sink or source processes (beside irrigation) that are not considered in NOAH model, hindered the reliability of the method in certain parts of the study area.

MW SM data alone, are also employed for detection of irrigation practices and its timing in different part of the world. Qiu et al., 2016 indirectly identified irrigated areas as they observe that, over eastern China, the increase in the soil moisture trend (by ESA CCI SM) cannot be explained by the trend obtained from the rainfall observations. Therefore, the increasing trend in soil moisture might be due to irrigation. Singh et al. (2016) used AMSR-E soil moisture data for discerning the shifting over time in the irrigation practices in north western India that was due to the Water Act implementation (after 2009) imposing restrictions on early (pre-monsoon period) cultivation of rice. A shift of two weeks in the onset of irrigation season was observed in the SM variation pattern. A recent study by Lawston et al. (2017) over three vastly irrigated areas in the United States also demonstrated that the spatial signature and seasonal timing of the irrigation can be identified using SMAP enhanced 9 km product.

Most of the above mentioned studies were focused on irrigation mapping. However, the assessment of water amounts used for irrigation, as opposed to simply mapping irrigated areas, is a much more difficult and complex task. Typically, irrigation amount is estimated by water balance models, and satellite observations (e.g., evapotranspiration) are used as additional inputs to constrain and calibrate the models (Droogers et al., 2010). By way of example, Peña-Arancibia et al. (2016) used MODIS data to estimate actual evapotranspiration (ETa) that is employed in a water balance model to estimate the amount and the source of irrigation in a basin in Australia. Estimating latent heat flux as the residual term in energy balance equation, is another approach to estimate crop consumptive water use that is related to the irrigation. However, large number of input data and the complexity of the methods from one side, and the clear sky precondition for running the model from the other side, hinder the practical application of these models (Kalma et al., 2008). Moreover, these method only provide the consumptive water use (i.e. the amount of water that is evaporated by the crop or from the soil), not the amount of the irrigation that is applied to the field. Differently, microwave (MW) satellite sensors can measure the soil moisture change in top soil layer effectively (operating in all-weather condition and using limited number of ancillary data) and might be a good solution for estimation of irrigation water use. However, up to now most of the studies has used MW sensors for the irrigation mapping (e.g. Escorihuela and Quintana-Seguí, 2016; Kumar et al., 2015; Lawston et al., 2017; Qiu et al., 2016) which is not considered as their strength due to the coarse spatial resolution of soil moisture products.

In this study, we propose an innovative approach that allows us to estimate irrigation water amount from satellite soil moisture data. Specifically, we exploit the SM2RAIN algorithm that was originally developed by Brocca et al. (2014) for estimating rainfall from the knowledge of soil moisture observations. The SM2RAIN method has been successfully applied for rainfall estimation on a regional (Brocca et al., 2013; Brocca et al., 2016; Ciabatta et al., 2017) and a global (Brocca et al., 2014; Koster et al., 2016) scale by using satellite soil moisture data. As the SM2RAIN algorithm estimates the total water entering into the soil, over irrigated regions it provides an estimate of rainfall plus irrigation. By the knowledge of rainfall from additional information (e.g., rain gauges or satellite precipitation products), or by assuming rainfall equal to zero (e.g., in dry periods over arid regions), the actual amount of irrigation water can be obtained.

The main objectives of this paper are as follow: (i) Assessing the capability of different SM product for detection of irrigation and selection of the best product in the region; (ii) Detection of irrigation signature (consistent with local irrigation practices) in time evolution of the selected SM product; and (iii) Estimation of irrigation using SM2RAIN method and satellite SM data and Evaluating the model performance in irrigated pixels against in situ irrigation and non-irrigated pixels.

2. Method

2.1. Simulating the total water entering the soil using SM2RAIN

The SM2RAIN algorithm was initially developed to estimate rainfall based on the water balance equation and the fluctuation of soil

moisture in time, by assuming that irrigation is not significant. However, over irrigated regions, SM2RAIN provides an estimation of total water entering into the soil, i.e., rainfall plus irrigation. Specifically, the soil water balance equation can be described by the following equation (Brocca et al., 2015):

$$nZ\frac{dS(t)}{dt} = I(t) - g(t) - r(t) - e(t) \quad (1)$$

where n [−] is the soil porosity, Z [mm] is the soil layer depth (n times Z is denoted as the Z^* that is the soil water capacity), $S(t)$ [m^3/m^3] is the relative saturation of the soil or relative soil moisture, t [day] is the time, $I(t)$ [mm/day] is the total water entering into the soil, i.e., rainfall plus irrigation, $g(t)$ [mm/day] is the drainage (deep percolation plus subsurface runoff) rate, $r(t)$ [mm/day] is the surface runoff and $e(t)$ [mm/day] is the actual evapotranspiration (ET_a).

Then to solve the equation for estimating the $I(t)$ the following assumptions are made:

1. The rate of surface runoff is negligible (see Brocca et al., 2015 for more details)
2. The drainage rate is related to the soil moisture through a power law equation, $g(t) = aS(t)^b$ (a and b are the drainage parameters)
3. ET_a is linearly related to potential evapotranspiration (ET_{pot}), $e(t) = ET_{pot}(t)S(t)$,

Applying these assumptions the Eq. (1) can be written as:

$$I(t) = \frac{Z^*dS(t)}{dt} + aS(t)^b + ET_{pot}(t)S(t) \quad (2)$$

where Z^*, a and b are three parameters to be estimated.

It is noteworthy that when actual ET (ETa) is available it can be used directly in the Eq. (2) instead of $ET_{pot}(t) \times S(t)$.

2.2. Estimating the irrigation amount

By using observed rainfall data, $P(t)$, or by assuming rainfall equal to zero (e.g. in dry periods), the actual amount of irrigated water, $IR(t)$, can be obtained using Eq. (3):

$$IR(t) = I(t) - P(t) = \frac{Z^*dS(t)}{dt} + aS(t)^b + ET_{pot}(t)S(t) - P(t) \quad (3)$$

In this study, we also considered the case in which the ETa data is available (Eq. (4)).

$$IR(t) = I(t) - P(t) = \frac{Z^*dS(t)}{dt} + aS(t)^b + ET_a(t) - P(t) \quad (4)$$

In Eqs. (3) and (4), $IR(t)$ is the average irrigation water depth [mm/day] at the pixel level. Note that when this value is negative it is assumed equal to zero.

To obtain the model parameter values (a, b and Z^*), the SM2RAIN algorithm is calibrated against reference rainfall data. Concretely, irrigation periods are masked and the model is calibrated during the non-irrigated period. This is done because during the irrigation seasons, the change in the SM is a result of both rainfall and irrigation; however, unlike rainfall, the ground truth irrigation data are not usually available. Thus, during the irrigation period the soil moisture fluctuation is not compatible with the rainfall pattern and the calibration would result in estimation of wrong model parameters. We also choose to calibrate the model using 10-day accumulated rainfall, as the best model performance in simulation of the precipitation over the region is obtained at this time step. So in this study, the minimization of the root mean square error (RMSE) between reference and simulated 10-day accumulated rainfall is chosen as the objective function for the calibration (for more details on the calibration process refer to Brocca et al., 2014, 2016).

2.3. Performance assessment

The assessment of the estimated irrigation water use is carried out by using two approaches: 1) The comparison of the simulated and the in-situ irrigation water use at monthly time step: indeed, the estimated irrigation is in terms of water depth (mm), so first the total volume of allocated irrigation water to the plain is divided by the plain area (i.e. 975 km^2) to estimate the in situ irrigation depth. Then, the total estimated irrigation depth at each pixel is divided by the fraction of irrigated area at that pixel (obtained from the land use map) to estimate the irrigation depth that is applied to the cropland area. Then, assuming that the whole plain is uniformly irrigated, the in situ and the simulated irrigation water use are compared in each pixel. Another approach for validation of results would be estimation of irrigation at all pixels that cover the plain and comparing the average estimated depth with the in situ irrigation depth. However, as it is explained in the Data collection section, due to some limitations at some pixels such as, data gap in soil moisture time series and presence of other irrigated area without in situ irrigation record, this approach is not considered in this study.

2) The retrieval of irrigation water in the non (less)-irrigated pixels close to irrigated pixels: The agreement between observed and estimated irrigation in the irrigated pixels and the estimation of nearly zero irrigation in the non-irrigated pixels can be consider evidence for good performance of the method in quantifying the irrigation water. The adjacent pixels are chosen to make sure the climatic condition is almost the same and the only factor that is changed is the irrigated area of the pixel.

2.4. Removing bias from SM2RAIN-estimated irrigation

Since the SM2RAIN-estimated irrigation and the observed rainfall might show systematic discrepancy where no irrigation is applied, the model bias is estimated over non-irrigated or rain-fed cropland areas and used for correcting the simulation at the irrigated pixels. Indeed, by removing the bias from the difference between the total water entering the soil (I) and the observed precipitation (P), we single out the differences due to the irrigation practices (Eq. (5)).

$$IR(t) = I(t) - P(t) - bias \quad (5)$$

To achieve this the monthly bias that is estimated over non-irrigated pixels is removed from the irrigation estimated at the adjacent irrigated pixel. Choosing the neighboring pixels for bias correction will maximize the possibility of the climate similarity, thus any difference in the estimated irrigation at the pixels can be attributed to the model bias rather than different rainfall pattern.

3. Study area and materials

3.1. Study area

The Miandoab plain is located in the southern part of Urmia Lake (one of the largest salt water lakes on earth and a highly endangered ecosystem) in west Azarbayjan province of Iran (AghaKouchak et al., 2015) (Fig. 1) and it is one of the main agricultural plains of Iran (Salmon et al., 2015). The climate of the region is semi-arid. In summer the rate of actual evapotranspiration (ET_a) is high and surface and ground water resources are used as supplemental resources alongside precipitation. Most of rainfall in this region occurs from January to May. Based on a 50-year record (1960–2010), the average annual precipitation and temperature are 296 mm and 12 °C respectively (ranging from −10 °C in December to 30 °C in August). Accordingly, the mean annual potential evapotranspiration (ET_{Pot}) is 900–1500 mm (Bagheri et al., 2017) and most of the irrigation occurs in spring and summer (April–September) (data from Meteorological Organization of Iran, www.irimo.ir).

The main surface water resources to irrigate this plain are the

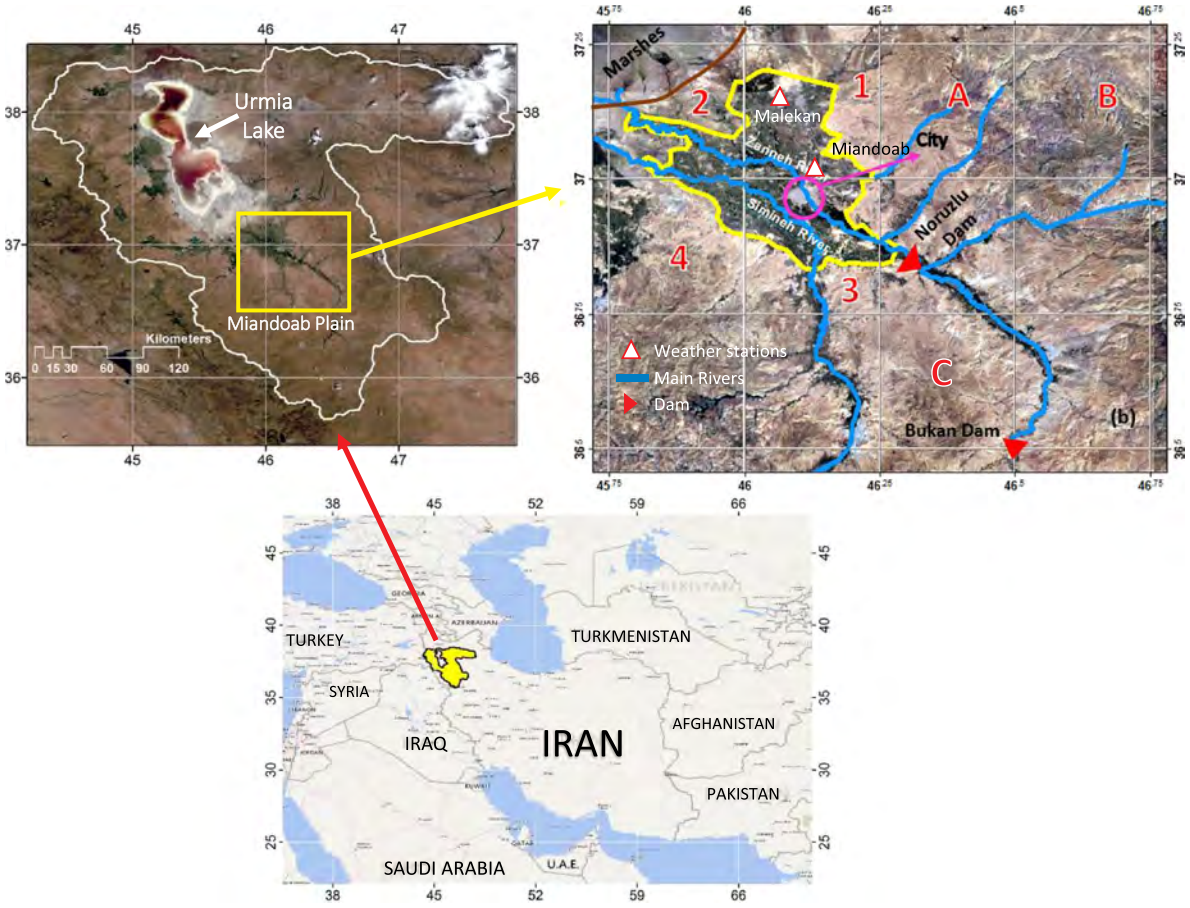

Fig. 1. Location map and overview of the area. a) The Urmia basin location in Iran. b) Urmia basin, Urmia Lake, the weather stations (Malekan and Miandoab) and the Miandoab plain in West Azarbayjan province of Iran. c) The Miandoab plain (yellow border), two main rivers and AMSR2 soil moisture grid cell located on the plain (pixel1–4, Pixel (A), Pixel (B) and pixel (C)). The Zarineh Rood River is the most important surface water resources for the Urmia Lake that supplies irrigation network of the plain through Norouzloo diversion weir. (For interpretation of the references to colour in this figure legend, the reader is referred to the web version of this article.)

Zarrineh-Rood and Simineh-Rood rivers that, after supplying the plain, reach the lake. Approximately, half of the input surface water to the Urmia Lake (almost 2 billion cubic meter per year) pass through this plain (Mahab Ghodss Consulting Engineering Co, 2010). The Urmia lake area has declined dramatically in last 20 years. This decline is mainly due to the diversion of water for irrigated agriculture (Pengra, 2012). The surface water from Zarrineh-Rood River is stored in Bukan Dam with the storage capacity of 834 million cubic meter, and then diverted to the irrigation network of Miandoab plain through Norouzloo diversion weir (Yekom Consulting Engineers, 2016). However, the surface water is only delivered effectively in two parts of the plain (i.e. North east (NE) and south East (SE)) with completed irrigation network (see Fig. 2), in other parts, due to lack of either main or secondary canals the surface water is not regularly provided and groundwater is used as a supplemental resources (Forootan et al., 2014; Tourian et al., 2015). The NE part of the irrigation network receives almost 30% more water than the southern part. Indeed, the direct (illegal) water extraction from the Simeneh Rood River and pumping from the ground water, are other resources for irrigation in the SE of the plain. The irrigation network supplies agricultural parcels of 20–60 ha, which due to lack of storage facilities in most cases are irrigated right after receiving water allotment (Yekom Consulting Engineers, 2016). The field application irrigation efficiency in the region is 30% predominated by surface irrigation (Hassanzadeh et al., 2012).

The volume of the water that is released from Norouzloo diversion weir to the irrigation network is recorded on monthly basis and used as the in situ irrigation data. Indeed, the volume of the irrigation water is divided by the irrigated cropland area of the Miandoab plain (i.e. 975 km^2) to estimate the in situ area-averaged monthly irrigation depth and then it is compared with the accumulated monthly irrigation depth estimated by SM2RAIN. It is also noteworthy that Miandoab plain is the only plain in the region that has irrigation network and a record of surface irrigation water volume. Thereby validating the method in other part of the case study is not possible. Nevertheless, the irrigation data in this plain is only accounted for the surface irrigation and there is no precise information about the volume of water withdrawal from wells or rivers for irrigation.

Based on the land use map of Urmia basin for year 2013, the total cultivated area of Miandoab plain is approximately 975 km^2 (Youneszadeh Jalili et al., 2017). The main crops in this plain are wheat, barley, potatoes, tomatoes, sugar beets, alfalfa and apples, in which wheat, barley are typically planted in October and harvested in June and the remaining are usually planted around April and harvested in October (Zaman et al., 2016). Since most of the crops in the region are irrigated between April to October and there is almost no rainfall in this period (the change in SM is mainly due to the irrigation), we consider April to October as the irrigation season in this study.

3.2. Data collection

The SM2RAIN algorithm uses soil moisture and actual evapotranspiration (ET_a) as input data. Precipitation data are also needed for calibrating the algorithm parameters.

The level 3 (L3) soil moisture product from Advanced Microwave

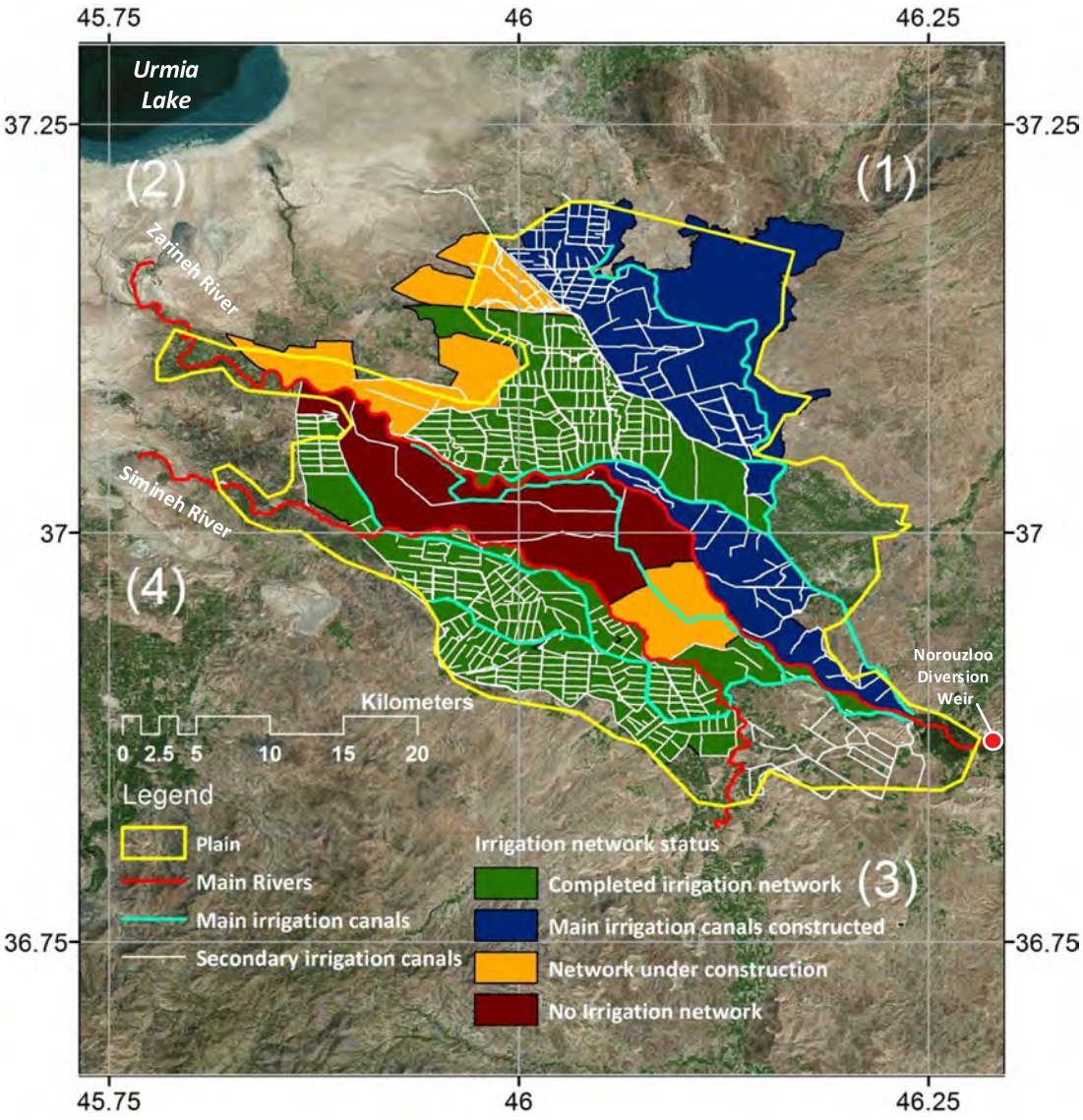

Fig. 2. Irrigation network in Miandoab plain; the red lines shows the main rivers (Zarineh and Simineh), the main and secondary irrigation canal are shown by cyan and white lines. The water is supplied from Norouzloo diversion weir to the main canals and deliver to the field through secondary canals. The zones with completed irrigation network (Green), only main irrigation canals constructed (Blue), Network under construction (Orange) and without irrigation network (red) are shown in the map. The AMSR2 grid cell location (pixel 1–4) are also indicated by the numbers in the map. (For interpretation of the references to colour in this figure legend, the reader is referred to the web version of this article.)

Scanning Radiometer 2 (AMSR2) at daily time scale and spatial sampling of 0.25 degree (~25 km) (Koike, 2013), for 4 years (July 2012–December 2015) is used as satellite soil moisture products in this study. We note that we performed a preliminary analysis (not shown for brevity) by considering different satellite soil moisture products and algorithms: ASCAT; SMOS; AMSR2 JAXA (Japan Aerospace Exploration Agency) AMSR2-LPRM (Land Parameter Retrieval Model), i.e., the AMSR2 soil moisture product obtained with JAXA and LPRM algorithms, respectively. Some of these products have specific issues in the investigated area. For instance, the number of soil moisture retrieval in SMOS is quite low due to radio frequency interference (RFI) problem (see Fig. S1 in the Supplementary material) and volume scattering in ASCAT causes an increasing pattern in SM during the dry season (here irrigation season) specially at pixels with low vegetation density (see Fig. S2 in the Supplementary material and Wagner et al., 2014). The above issues are not observed in AMSR2 SM time series. Among AMSR2 SM algorithms (i.e. JAXA and LRPM), the JAXA data is reported to have a closer SM dynamic to the in situ data and a better performance in the arid and semi-arid area compared to LRPM (Bindlish et al., 2018; Kim et al., 2015). Therefore, AMSR2-JAXA soil moisture dataset is employed in this study for estimation of the irrigation water use. The AMSR2-JAXA soil moisture dataset is available online through GCOM-W1 Data Providing Service: https://gcom-w1.jaxa.jp. Since the Ascending (13:30) overpass is usually closer to the irrigation time in the plain, the analysis is done using this product only. Additionally, soil moisture observation characterized by low quality (e.g., frozen/snow conditions, pixels near coastal area, big lakes and marshes, dense forest and big urban area) are removed from the dataset.

The Miandoab plain is covered by four pixels of AMSR2 (Fig. 1). The evaluation of the quality and accuracy of soil moisture data, based on the aforementioned criteria, shows that the soil moisture retrieval at Pixel (2) is frequently flagged unreliable due to presence of lake water body and marshlands in large fraction of this pixel (see Fig. S3 in the Supplementary material). Similarly, in Pixel (3) a large urban area (the Miandoab city) is present (see Fig. S4 in the Supplementary material) that can have an impact on the accuracy of the soil moisture retrievals, however; since the size of the city is small compare to the pixel area this pixel is kept in the analysis. Pixel (4) covers two irrigated cropland plains (including

Table 2
The properties of the AMSR2 pixels that cover the Miandoab plain and the surrounding non-irrigated area.

Pixels	Fraction of irrigated area	Fraction of the area with the well-established irrigation network to the total irrigated area at each pixel	Note
1	0.49	%80	Most of the irrigation water at this pixel is coming from the irrigation network
2	0.20	%15	This pixel is the closest to the Urmia lake and partly covered by the marshland. The irrigation network is mostly under construction at this pixel.
3	0.47	%60	Simineh Rood river and ground water resources are used as the supplemental resources to the irrigation network at this pixel
4	0.17	Not known	This pixel covers two irrigated plain. There is no information about the irrigation network in the western plain
A	< 0.10	0	Two rivers cross this pixels and small irrigated area can be seen around them
B	0.02	0	The pixel is located in the hillside and the irrigated croplands are scattered and small
C	< 0.05	0	Some irrigated area can be seen at NE part of the pixel where Zarineh Rood river cross the pixel

Miandoab) with different irrigation system. As it is not possible to separate the irrigation water of each plain from the average soil moisture retrieval, we do not compare estimated irrigation at pixel (4) with the observed data, however; the amount of irrigation in this pixel is still estimated for the reference (see Fig. S5). As a result, in this study irrigation will be estimated at Pixel (1) and pixel (3) and will be evaluated against in situ irrigation data and non-irrigated pixels. Three neighboring pixels (pixel A, B and C in Fig. 1) with almost no irrigated area are chosen as the non-irrigated pixels to be compared with pixel 1 and 3. A summary of the fraction of irrigated area and well-established irrigation paddocks and conveyance system at each pixel is shown in Table 2.

The 10-day averaged ET_a product estimated by the ET look algorithm (Bastiaanssen et al., 2012) through Penman-Monteith equation that is provided by FAO: Water Productivity Open-access portal (WaPOR) for Africa and near east with 250 m spatial resolution is used as input evapotranspiration product (https://wapor.apps.fao.org). However, reliable ET_a product is not always available, thus in this study a simpler method is also used in which ET_a is estimated as a linear function of ET_{pot} and soil moisture (hereafter SM_ETp(GLEAM)). The ET_{pot} is obtained from Global Land Evaporation Amsterdam Model (GLEAM v3.1, Martens et al., 2017) that provides the daily Potential evapotranspiration data based on the Priestley and Taylor equation with 0.25° spatial resolution.

Daily observed precipitation data from 2012 to 2015 are obtained from two weather stations that are operated by the Meteorological Organization of Iran (www.irimo.ir) (see Fig. 1 for their location) and their arithmetic mean daily precipitation is used as the in situ precipitation data. In addition, the Multi Source Weighted Ensemble Precipitation (MSWEP) product obtained by merging gauge, satellite, and reanalysis data that is globally available at 3-hourly time steps and 0.25° spatial resolution from 1979 to 2015 is considered (Beck et al., 2017) to assess the model performance where reliable ground observations are not available.

The allocated water to the irrigation network from the Norouzloo diversion weir is obtained from Iranian Water resources management company (IWRM co., http://portal.wrm.ir). The data is reported on the monthly basis (from June 2012–December 2015) and provided in million cubic meters (MCM) of the water that is released to the irrigation network. The data is converted to the depth of irrigation (mm) by dividing to the plain irrigated cropland area (i.e. 975 km^2). Since the canals are mostly lined with concrete we neglect any water loss in the conveying system and assume that the whole amount of the released water is delivered to the field. A brief summary of the datasets used in this paper is shown in Table 3.

4. Results

In this section, we present the results for the quantification of irrigation water use in Miandoab plain from AMSR2-JAXA soil moisture data via SM2RAIN algorithm. Then, we compare the retrieved irrigation water with observed irrigation data, and we evaluate the model performance in less-irrigated regions. The results are first presented without removing the false irrigation and then the bias-corrected irrigation are shown and discussed in Section 4.4.

4.1. Rainfall estimation through SM2RAIN in non-irrigated periods

Before estimating the irrigation, the skill of SM2RAIN in simulation of precipitation is evaluated. This is important because the errors in rainfall estimation can be propagated to our irrigation estimates. In Fig. 3 the SM2RAIN-estimated rainfall plus irrigation depth at pixel 1 and 3 (using Eq. (4)) is compared with the ground-based rainfall data for the period 2012–2015 (see Fig. S6 of Supplementary material for the simulation with Eq. (3)). In the bottom panel, the soil moisture time series from AMSR2-JAXA is also illustrated. The highlighted areas are masked out as they are periods in which irrigation might occur. The non-zero simulated rainfall plus irrigation in these periods is an evidence that the proposed approach can capture the irrigation signal. Outside the irrigation season there is a good agreement between estimated and observed rainfall (see Table 4). In particular, using different rainfall dataset for calibration, return almost the same results in pixel (1) with MSWEP performing slightly better, however, using gauge precipitation data for calibration in pixel (3) is resulted in substantial improvement in the model simulation. On the other hand, employing different ET dataset has nearly no impact on the rainfall simulation as the rate of ETa is negligible during the precipitation (this is only true when the irrigation seasons are masked). (See Table 4.)

4.2. Determination of irrigation water in agricultural areas via SM2RAIN

To determine the amount of irrigation water use, the differences between monthly simulated water entering into the soil (irrigation plus rainfall) and monthly observed rainfall is computed. The upper panel in Fig. 4 illustrates, the monthly rainfall plus irrigation when gauge (Fig. 4a) or merged satellite-gauge products (Fig. 4b) are used as the reference rainfall for model calibration. Accordingly, the lower panel shows the simulated irrigation that is simply the difference between simulated and observed rainfall. The simulation performed by adopting different ET products are also shown by red and blue dashed lines in this Figure.

Using less sophisticated ET algorithm (SM_ETp(GLEAM)) in Eq. (3) results in underestimation of ETa and consequently irrigation water use (see Fig. S7 in the Supplementary material). Indeed, in this situation the model mainly depends on the change in the soil moisture (see Figs. 5 and 6 for contribution of each term to the estimated irrigation), but it is still able to capture the irrigation seasonality consistent with the in situ data. On the other hand using WaPOR ET_a dataset almost always lead to higher estimate of the irrigation (see Fig. 4c and d). This can be attributed to not considering supplementary water resources (groundwater or direct water extraction from the rivers) in the in situ irrigation

Table 3
Summary of the datasets used in this study.

Datasets	Agency producer	Spatial extension	Period	Spatial/temporal sampling
GLEAM	ESA	Global	2011–2015	0.25°/1-day
AMSR2	JAXA	Global	2012–continuing	0.25°/~1-day
WaPOR	FAO	Africa and near east	2009–2017	250-m/every 10 days
MSWEP	European Commission, Joint Research Centre (JRC)	Global	1979–2015	0.25-degree/3 h
In-situ Precipitation	Meteorological Organization	–	1980-continuing	1-day
In-situ irrigation	WRM organization	–	2012–2015	Monthly

dataset. However, according to the recent technical report by Yekom Consulting Engineers, (2016) around %80 of water demand in pixel (1) is supplied by the irrigation network, thus in situ data should be a good representative of irrigation at this pixel. Another possibility is a systematic overestimation by the model that is investigated in Section 4.4. Indeed, the estimated irrigation at a non-irrigated pixel (false irrigation) is used to disentangle the irrigation signal from the model bias and then bias-corrected irrigation is compared against the in situ data.

The lag between simulated and observed irrigation at the start of the irrigation seasons, when MSWEP precipitation data is used (Fig. 4d) can be related to overestimation of this product at the beginning of the spring (April and May). On the other hand during this period despite the release of the water for the irrigation there are still some rain events in the region that can overshadow any soil moisture changes triggered by the irrigation, thereby a general underestimation is expected.

The time average contribution of each term to the total simulated rainfall plus irrigation are calculated for the 6 pixels (3 irrigated and 3 non-irrigated) over irrigation seasons and are shown in the Fig. 6. The major contribution, when Eq. (4) is used, is made by ET term with an average value of 65%, followed by the soil moisture variation term ($Z^* ds/dt$) with average value of 35%. This highlights the importance of considering soil moisture variation alongside sophisticated evapotranspiration algorithm for irrigation estimation. The contribution of the drainage term (as^b) is negligible ($< 5\%$); however, during the rainy seasons, when the soil moisture is close to the saturation (usually after rainfall), it plays a more important role in the SM2RAIN simulation. It is also expected that by using a higher resolution SM product, soil

Table 4
The model performance in simulating precipitation in terms of R, RMSE (mm/day) in pixel (1) and 3 (Irrigation period is masked); using a better rainfall dataset for model calibration can have a significant impact on the simulation outcome (as in pixel 3), but the model seems insensitive to the input ET dataset.

ET data	Precipitation data			
	Pixel (1)		Pixel (3)	
	In situ	MSWEP	In situ	MSWEP
ETa (WaPOR)-Eq. (4)	(0.66, 1.03)	(0.69, 0.99)	(0.76, 0.87)	(0.63, 1.33)
ETpot (SM_ETp(GLEAM))-Eq. (3)	(0.65, 1.02)	(0.69, 1.04)	(0.76, 0.87)	(0.6, 1.38)

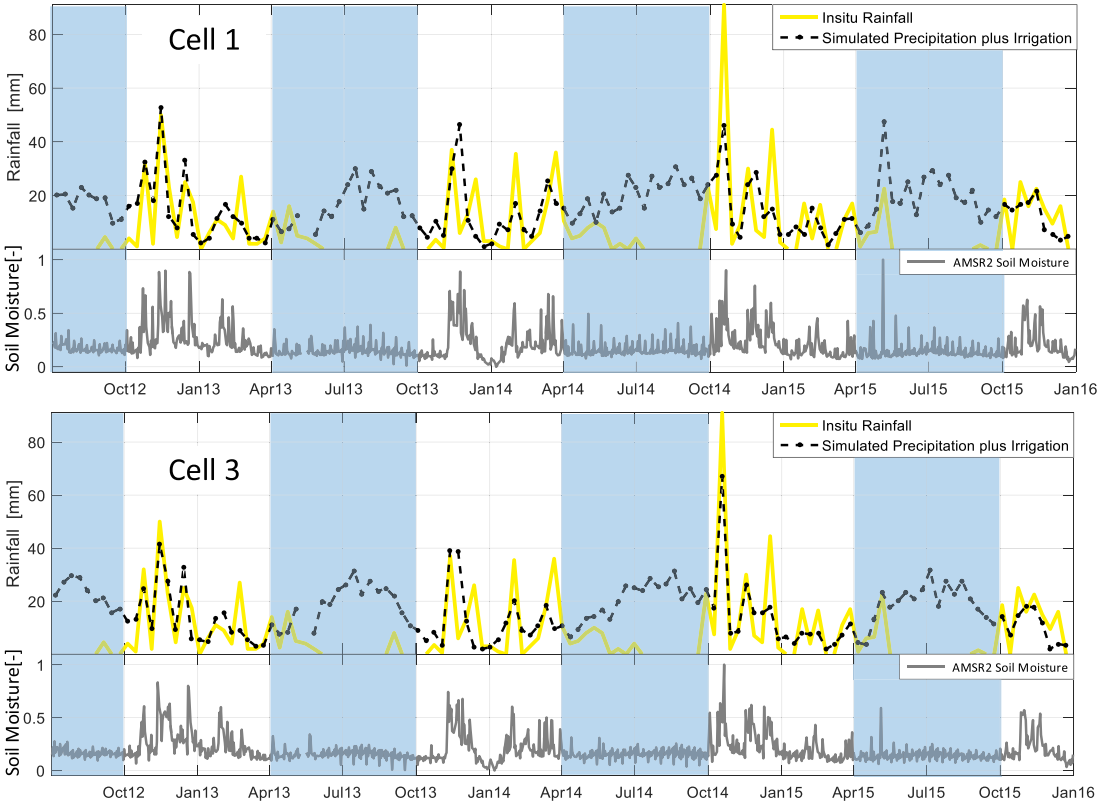

Fig. 3. Simulation of 10-day rainfall plus irrigation from SM2RAIN (Eq. (4)) and comparison with ground-based rainfall in pixel (1) (upper Figure) and pixel (3) (lower Figure). In the upper panel of each plot the estimated rainfall plus irrigation and observed rainfall is illustrated, in the lower panel the relative soil moisture time series from AMSR2-JAXA is shown. The highlighted areas are masked out as they are the periods in which irrigation might occur.

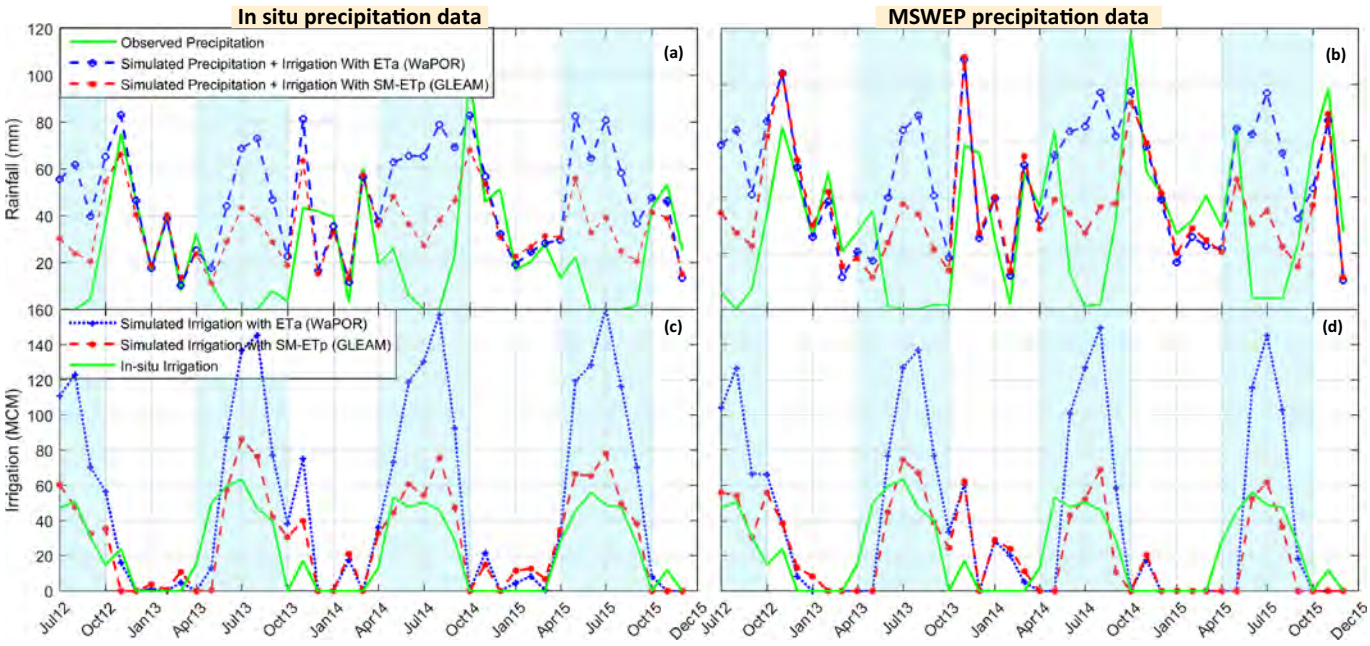

Fig. 4. The quantification of irrigation water of the plain, evapotranspiration impacts on the retrieved irrigation water depth and comparison of simulated and observed irrigation water of the plain. a) SM2RAIN estimate of precipitation plus irrigation using in situ precipitation data for calibration. b) SM2RAIN estimate of precipitation plus irrigation using MSWEP precipitation data for calibration. c) The simulated irrigation by SM2RAIN using in-situ precipitation data. d) The simulated irrigation by SM2RAIN using MSWEP precipitation data. The upper panel is showing observed precipitation (solid green line) and the simulated Precipitation plus irrigation of Pixel (1) using WaPOR ETa (Eq. (4)) and SM_ETp(GLEAM) data (Eq. (3)) (blue and red dashed lines respectively). The lower panel shows the comparison of retrieved and in-situ irrigation water. In this panel the evapotranspiration impacts on the retrieved irrigation is shown. Dashed blue and red lines are quantified irrigation water estimated by employing WaPOR ETa data in Eq. (4) and SM_ETp(GLEAM) data in Eq. (3), respectively. (For interpretation of the references to colour in this figure legend, the reader is referred to the web version of this article.)

saturation occurs more frequently and the drainage contribute more to the final estimated irrigation. Using Eq. (3) yields different results. Soil moisture variation term makes > 75% contribution (on average) to the total simulated rainfall plus irrigation; whereas, ET contribute < 25% (see Fig. 6a). In the non-irrigated pixels, regardless of which equation is used, both soil moisture variation and ET terms have almost the similar contribution to the estimated rainfall plus irrigation and drainage contribute around 15% on average.

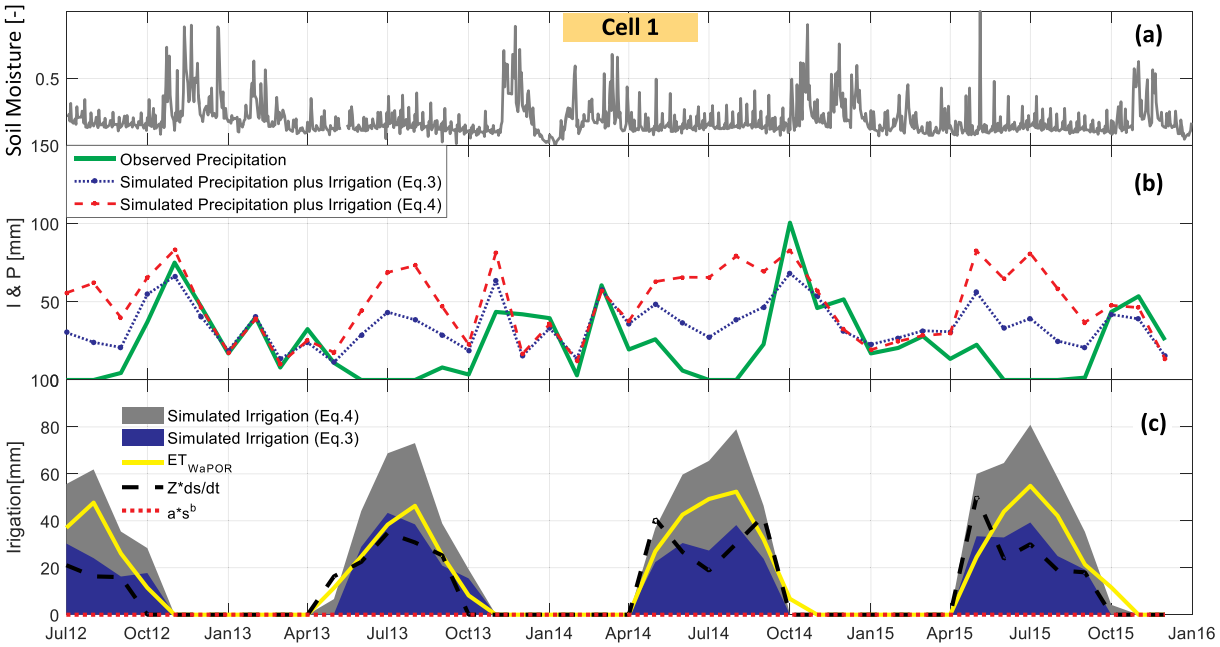

Fig. 5. Contribution of soil moisture variation term (Z^*ds/dt), drainage term (as^b) and ET term (ET_{WaPOR}) to the simulated irrigation in cell 1 during the irrigation season (i.e. April–October) using different irrigation estimation method (i.e. Eqs. (3) and (4)); (a) shows the soil moisture fluctuation, (b) shows the simulated precipitation plus irrigation that are estimated using Eqs. (3) and (4) and compares them with the observed precipitation, and (c) shows the estimated irrigation obtain from Eqs. (3) and (4) (the area graph) alongside the contribution of soil moisture variation term (Z^*ds/dt), drainage (as^b) and evapotranspiration (ET_{WaPOR}) terms.

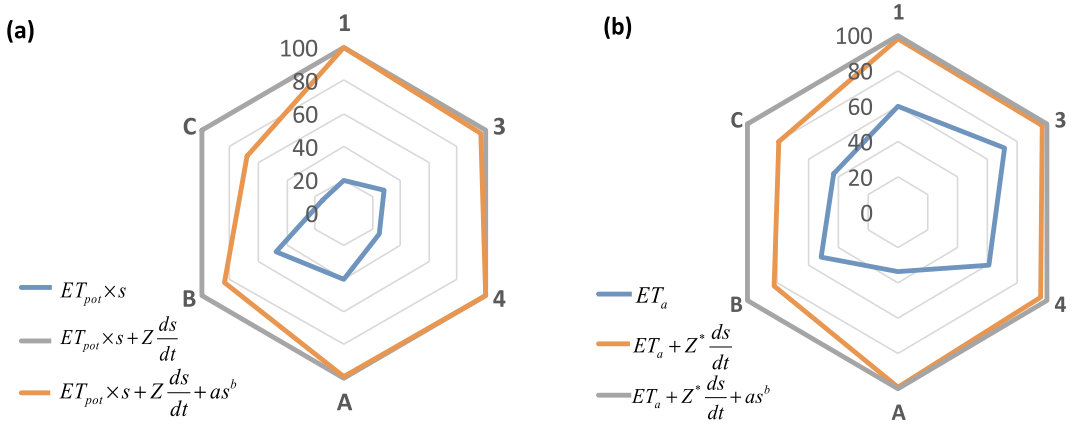

Fig. 6. - Percentage fraction of each term contribution to the estimated irrigation during the almost no-rain period (Apr-Oct) at 3 irrigated cells (1, 3 and 4) and 3 non-irrigated cells (A, B and C) when a) Eq. (3), and b) Eq. (4) is used for estimation of irrigation.

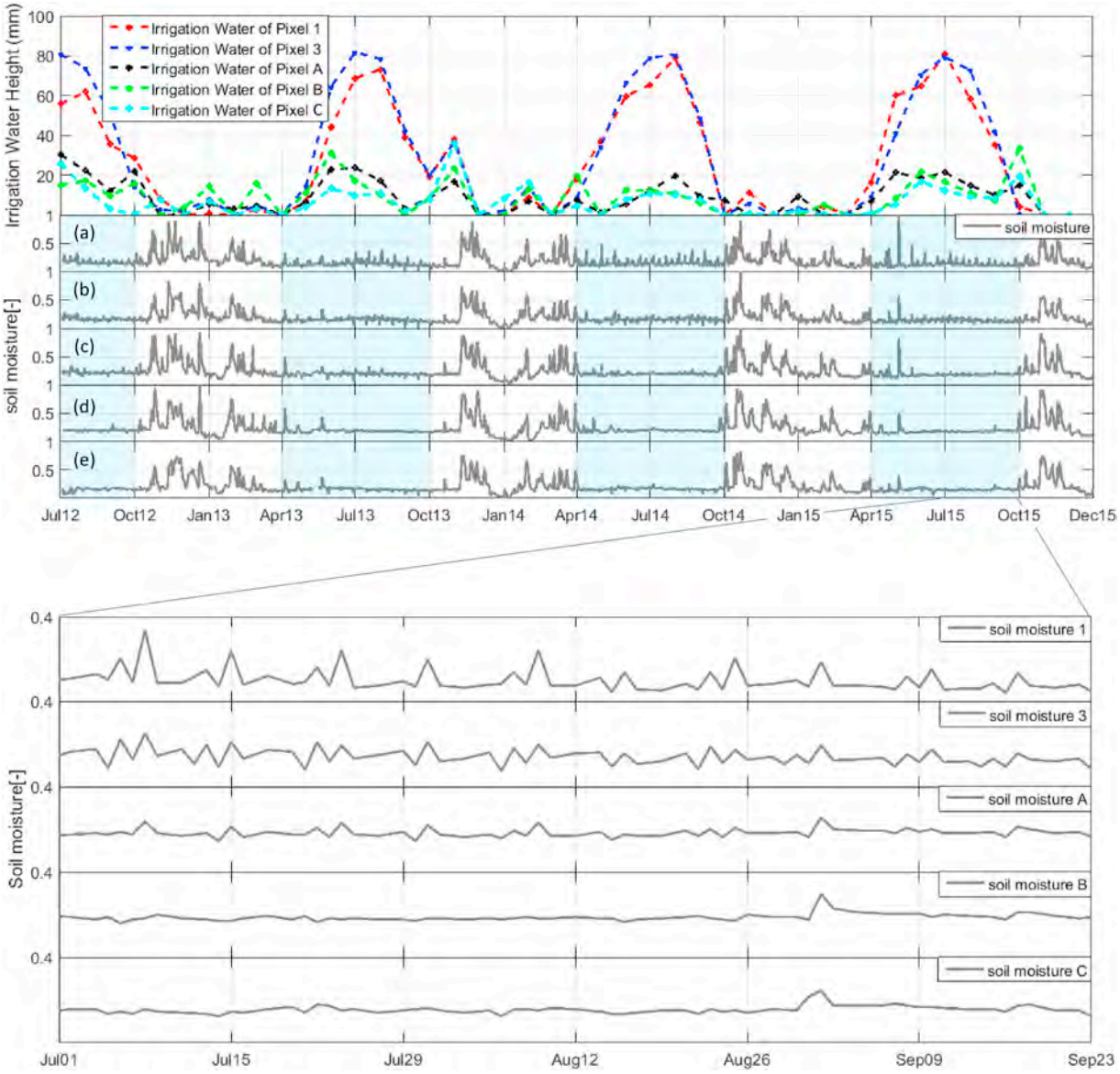

Fig. 7. Comparison of monthly irrigation water amount and soil moisture fluctuations in 5 pixels. a) Pixel (1), b) Pixel (3), c) Pixel (A), d) Pixel (B) and e) Pixel (C). The soil moisture fluctuations and irrigation water depth of non-irrigated Pixels (A), (B) and (C) in the highlighted period is considerably lower than irrigated Pixels (1) and (3). The barely visible soil moisture signal observed in pixel (A) in the lower enlarged Figure can be attributed to contribution of the neighboring irrigated pixels (especially pixel 1) to its signal, mainly due to low spatial resolution of AMSR2 soil moisture product.

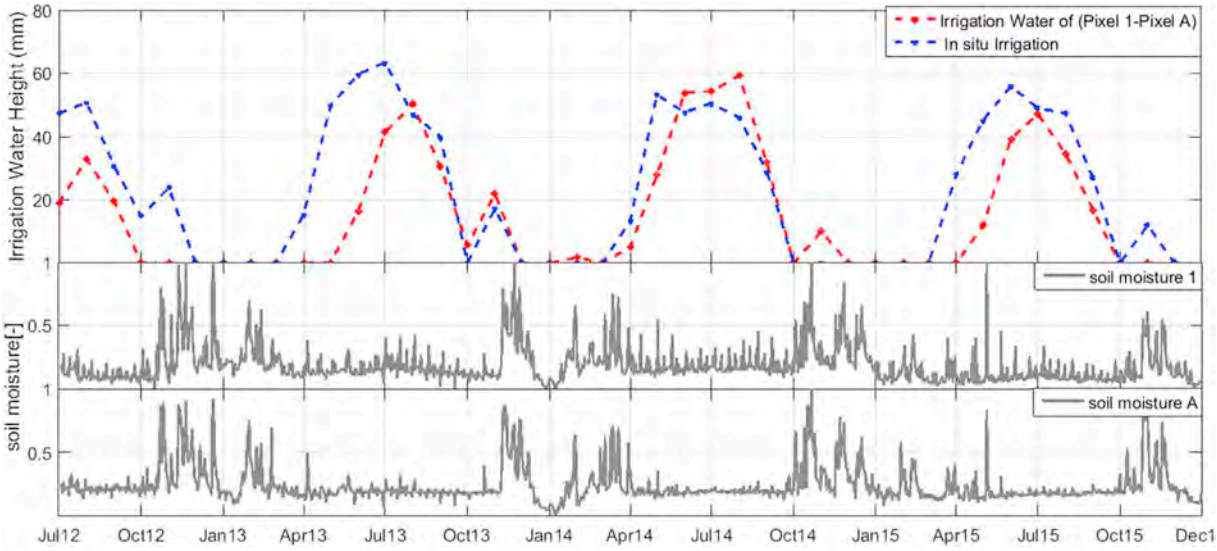

Fig. 8. The difference between estimated irrigation at pixel (1) (irrigated pixel) and pixel (A) (less irrigated adjacent pixel) and comparison with in situ irrigation data at the plain.

4.3. Assessment of the method in the non-irrigated areas

To evaluate the reliability of SM2RAIN algorithm, the simulation is also conducted over sparsely irrigated areas. To this end, the estimated irrigation water use in Pixel (1) and (3) (the irrigated pixels), that is obtained by adopting WaPOR ETa in Eq. (4) and using gauge precipitation as the reference rainfall, is compared with the three adjacent pixels with less irrigated area (Pixel (A), (B) and (C)). Fig. 7 shows the comparison of soil moisture fluctuations and monthly simulated irrigation water depth in the five pixels. As it can be seen, the monthly irrigation in Pixel (A), (B) and (C) is considerably lower than Pixel (1) and (3), although it is not completely zero, likely due to the noise in soil moisture retrievals and to the spatial resolution of AMSR2 (equal to $62 \times 35\ km^2$). Indeed, even though the AMSR2 data are mapped onto a regular 25 km grid, the neighboring pixels contribute to the signal and also Pixel (B) is partly affected by irrigation. This bias observed in the non-irrigated pixels are used to correct the model simulation at the irrigated pixels as it is explained in the Sections 2.4 and 4.4.

In the irrigated pixels a weekly signal is detected in the soil moisture fluctuations that is consistent with the common irrigation practices in the region. The estimated irrigation at Pixel (1) and (3) is always larger during the irrigation seasons. However; at the start of the wet season there are some irrigation estimated in the non-irrigated pixels that is likely due to error in ground-observed precipitation data (few reliable rain gauge stations are available near Miandoab city). Applying the method in a region with denser rain gauge network might result in a better simulation (this is further discussed in the Section 5.1).

4.4. Correction for the bias calculated over non-irrigated pixels

If we assume that the irrigation estimated at a non (less)-irrigated pixel is a model error, then to isolate the irrigation practices signal, the SM2RAIN-estimated irrigation must be corrected for this bias. Thus, using Eq. (5), the irrigation estimated at adjacent less-irrigated (or non-irrigated) pixels (pixel A and C respectively) are subtracted from the estimated irrigation at pixel 1 and 3 (irrigated pixels).

It seems that the bias-corrected irrigation at pixel 1 and 3 is better matched with the in situ irrigation data (see Figs. 8 and 10 and Table 5), however; in pixel (1) the irrigation seems to be under estimated in year 2012, 2013 and 2015. This can be explained in part by the fact that pixel (A) is not completely non-irrigated, indeed there are some irrigated areas in regions close to the rivers in this pixel (see Fig. 1). Moreover, as it is mentioned in the previous section it is expected that the irrigated pixel (1) is also contributing to soil moisture signal at pixel (A). Thereby, it is possible that by removing the bias, true irrigation signal is removed from pixel (1). Another candidate for adjacent non-irrigated pixel for pixel (1) would be pixel (B), however; being located in a mountainous area with average height of 1963 m (almost 500 m higher than average height at pixel A) (based on SRTM DEM v2, Nasa jet propulsion lab (JPL), 2013), some over estimation in ETa is expected in this pixel which is a known issue for energy balance algorithms (Li et al., 2009). This overestimation in ET result in higher irrigation estimates at pixel (B) compare to pixel (A). Fig. 9 shows the ETa rate for pixel (1), pixel (A) and pixel (B) from WaPOR ET dataset along with ETpot at pixel (B) from GLEAM dataset (average of 10 days in mm).

Table 5
The statistics for bias-corrected simulated irrigation at pixel 1 and 3.

	RMSE (mm/month)	R
Irrigation Pixel (1-A)	13.14	0.84
Irrigation Pixel (3-C)	12.65	0.88

The bias-corrected irrigation at pixel (3) is better aligned with the in situ irrigation data but sometimes overestimates the irrigation (see Fig. 10 and Table 6). This can be partially attributed to the fact that only around 60% of the total irrigation at pixel (3) comes from irrigation network and the rest is from ground water and direct pumping from the rivers (Yekom Consulting Engineers, 2016) which are not included in the observed irrigation data, although they are captured by SM2RAIN. Besides, the non-irrigated pixel (C) is mostly surrounded by the less or non-irrigated areas, so it is expected that the SM signal at this pixel is less affected by the irrigated pixels i.e. pixel (3). The average noise (bias) to irrigation signal ratio at pixel 1 and 3 is 24% that is estimated during Apr-Oct of 2012–2015.

The same analysis using $SM\_ETp(GLEAM)_t$ dataset (Eq. (3)) is also carried out that result in underestimation of irrigation at pixel 1 and 3 (see Fig. S7 of the Supplementary materials), however; the simulated irrigation pattern is still consistent with the in situ irrigation data.

At the start of each irrigation period (Mar-May) an underestimation is observed in the model simulations. Indeed, despite the release of water from Dam for irrigation, there are still some rain events at the end of the winter and beginning of the spring (the highlighted area in Fig. 11) that decrease the difference between the soil moisture at the

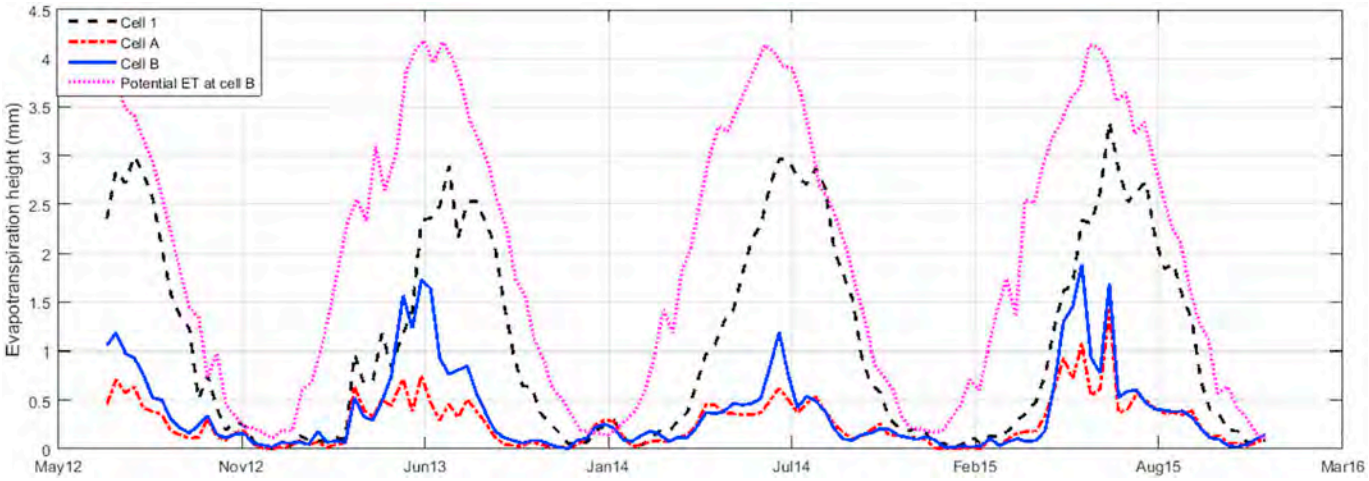

Fig. 9. 10 day averaged ETa at pixel (1), A and B based on WaPOR ETlook product, and 10 days averaged ETpot at pixel (B) based on GLEAM product; pixel (B) has the lowest cropland area among these three pixels but being located in a mountainous area and having lower temperature is usually misinterpreted by the energy balance algorithm as higher rate of ET thus pixel (A) is chosen as the non-irrigated pixel to be subtracted from pixel (1) to correct for the bias.

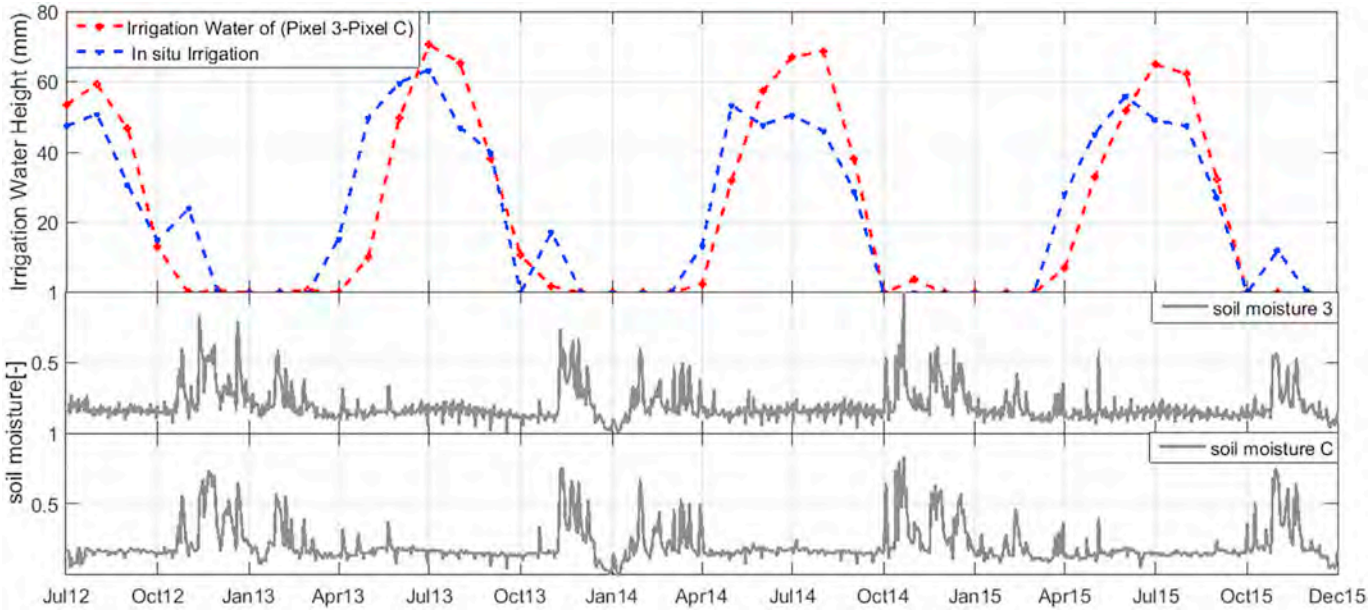

Fig. 10. The difference between estimated irrigation at pixel (3) (irrigated pixel) and pixel (C) (less irrigated pixel) and comparison with in situ irrigation data at the plain; the bias-corrected irrigation pattern shows good agreement with in situ data (better than pixel 1-A) the reason can be a bigger fraction of cropland in pixel (3) (compare to pixel 1) are using supplementary water resources (e.g. ground water) for irrigation whereas in situ irrigation data is only accounting for surface irrigation, thus higher estimated irrigation are expected.

irrigated and non-irrigated pixels, hence lower irrigation is estimated. There are also some cases where simulated precipitation in pixel (A) is bigger than pixel (1) (e.g. Oct 2014 and 2015) in which zero irrigation is reported.

5. Discussion

Different factors are influencing the estimated irrigation using satellite soil moisture data: 1) the quality of precipitation data, 2) the noise in the soil moisture data, 3) the choice of ET estimation method, 4) the amount of negative irrigation estimated by the model, and 5) the bias caused by spurious soil moisture signal and unknown fraction of irrigated area at each pixel. In this section, the limitation imposed by each of these factors are discussed.

5.1. The quality of the precipitation data

The impact of precipitation data on the irrigation estimates are twofold. The SM2RAIN estimates the total water entering the soil ($I(t)$) by first calibrating against precipitation data. Thus the density of rain gauge or the quality of precipitation product can have a great impact on the estimation of SM2RAIN parameter values. Two networks of precipitation stations are operating in the region; Iran Water resources management organization (IWRM) and the synoptic station of Islamic Republic of Iran Meteorological Organization (IRIMO). However, due to some discrepancy between their collected data (during the period of the study), only IRIMO network is considered which result in only two stations in the investigated region (Miandoab and Malekan). MSWEP is also used as another source of precipitation data to test the model. MSWEP is merging satellite, reanalysis and rain gauge data to estimate precipitation (Beck et al., 2017). As no station from Iran is included, it

is solely dependent on satellite and reanalysis data. The delay between retrieved irrigation using MSWEP products and observed irrigation water amounts in Fig. 4d can be partly explained by this problem.

$P(t)$ is also subtracted from $I(t)$ thus influencing the final IR (t) estimation. Specifically, in poorly gauged basin with high special variation in rainfall rate, over/underestimation might occur in the irrigation estimation. For instance, local precipitation around a station can introduce tremendous error to the model as soil moisture at the pixel scale would not increase, whereas, high rate of precipitation is recorded.

5.2. Noise in soil moisture data

It is well known that presence of the vegetation cover attenuate the soil moisture signal and decrease its quality (Jackson and Schmugge, 1991). Therefore, there is this possibility that the algorithm is not responding to the increased irrigation in Pixel (1) but rather to the noise generated by the denser vegetation cover in this pixel. To make sure that the observed signal in Pixel (1) is due to increase in soil moisture, the soil moisture variations at three adjacent pixels (i.e. Pixels (1), (A) and (B)) are compared during the wet seasons of 2014 and 2015. The result indicates that, when the main driver of the change is the same (i.e. precipitation) the same dynamic is observed in the soil moisture time series and the SM product is nearly insensitive to the vegetation cover (see Fig. 12).

On the other hand, a weekly signal is observed in soil moisture time series of Pixel (1) and (3) (see Fig. 7) that can be related to regular irrigation application in the plain, but another credible explanation can be the periodic error due to the orbital repeat cycle of the satellite (Su et al., 2013). However, according to the AMSR2 data user's manual the satellite repeats its original orbit every 16 days, whereas; a weekly signal is observed at Pixel (1) and (3). This periodic signal is also not observed in the non-irrigated pixels (Pixel (A), (B) and (C)) in the region (see Fig. 7). Moreover, according to the Iran water resources management organization (IWRM), the fields in Pixel (1) in the Miandoab plain are receiving water 2 times every 15 days from Norouzloo diversion weir, and thus it is probable that what is seen in the SM time series is driven by the irrigation application in the region.

Erroneous retrieval can be interpreted as spurious irrigation, thus pixels that are located in areas with complex topography, highly urbanized and close to water bodies should be removed from the analysis (Koike, 2013). SM2RAIN needs a strong soil moisture signal from the irrigation that can be received when a large fraction of the pixel is irrigated all within a short period of time (e.g. several days). For instance, most of the irrigation at pixel (1) is supplied from irrigation network which due to the lack of storage facilities at the fields (Yekom Consulting Engineers, 2016) is applied shortly after receiving the water allotment. Thus, large area of the pixel are irrigated in a short period of time (several days) and strong soil moisture signal (detectable by the satellite) is created. It is also possible that the irrigation method impact the model simulation. By way of example, the low efficiency irrigation methods like flood irrigation, can increase the soil moisture to a greater extent compare to drip irrigation, and hence, they are expected to be better captured by SM2RAIN. This interesting aspect will be investigated in the future studies.

5.3. The choice of ET estimation method

As it is explained in the Results section, ETa as a measure of consumptive water use makes a substantial contribution to the final estimated irrigation by SM2RAIN. In this study two ET dataset, i.e. SM_ETp (GLEAM) and WaPOR ETa, are adopted in Eqs. (3) and (4) respectively, to estimate the irrigation. Better results obtained using the WaPOR ETa in Eq. (4) as it uses more sophisticated and data-intensive algorithm while using SM_ETp(GLEAM) in Eq. (3) only lead to capturing the irrigation pattern. However, the results obtained by employing SM_ETp (GLEAM), the linear approximation, is also an important achievement because this equation (unlike the Eq. (4)) estimates the irrigation using limited number of ancillary data and mainly based on the SM observations. On the other hand, new data-driven approaches has been recently developed that can estimate ET based on the observed long-term negative changes in SM time series (e.g. Akbar et al., 2018; Koster et al., 2017; McColl et al., 2017). Thus the linear approximation, as the main source of uncertainty in Eq. (3), can be replaced by these ET parameterization techniques (called loss functions) and provides a stand-alone irrigation estimation method based on microwave soil moisture observation with higher accuracy.

5.4. Negative irrigation estimated by the model

Underestimation of rainfall by the model can result in estimation of negative irrigation. This usually occurs in wet seasons when no irrigation is applied to the fields. The negative bias can be a representative of the SM2RAIN precipitation simulation error that has a direct impact on estimating the irrigation. The comparison between the estimated negative bias (the model error) and positive bias (irrigation) in the irrigated pixels (1 and 3) shows that the average negative irrigation (SM2RAIN error) is less than a third of average positive irrigation which indicate the model has acceptable result in estimation of the irrigation (see Table 6).

Table 6
The estimated positive and negative irrigation (SM2RAIN error) in pixel 1 and 3 and also bias-corrected pixels i.e. (1-A) and (3-C), using in situ precipitation data and WaPOR ETa; in SM2RAIN model the estimated negative irrigation is set equal to zero, this simplification can introduce some error in the model estimates but since the average negative irrigation is almost one third of the average positive irrigation it would not have a considerable impact on the model outcome.

	Pixel 1	Pixel 3	Pixel 1 – Pixel A	Pixel 3 – Pixel C
Mean Negative Irrigation	−9.78	−10.74	−5	−8.49
Mean Positive Irrigation	35.42	38.37	22.4	25.82

5.5. The bias caused by spurious soil moisture signal and unknown fraction of irrigated area at each pixel

The spurious increase in soil moisture can be taken as the irrigation signal. In this study, it is assumed that the estimated irrigation at the largely non-irrigated pixels during the rainless irrigation period are caused by these spurious signal, thus the irrigation is corrected by subtracting the bias estimated in the largely non-irrigated adjacent pixels. However, the choice of non-irrigated pixel is crucial. It should share the same climate and rainfall pattern with the irrigated pixel, so that the true soil moisture signal in the non-irrigated pixel is not removed from the irrigated pixel (this issue can be addressed by selecting an adjacent non-irrigated pixel). However, presence of small fraction of irrigated area in the non-irrigated pixels is usually inevitable, furthermore; due to the coarse resolution of MW satellite (~50 *km*), the soil moisture signal in the non-irrigated pixel might be affected by the neighboring irrigated pixels. The choice of non-irrigated pixel with minimum cropland area that is mostly surrounded by the other non-irrigated pixels (as in Pixel C) can minimize the amount of the false irrigation signal in the non-irrigated pixels.

The other limitation is, in a general domain, the information about the potential locations of the irrigated areas may not be available. Thus, estimation of the average irrigation depth in the irrigated pixels and the detection of non-irrigated pixel would be difficult. This problem can be overcame, to some extent, by using global irrigated area map (e.g. (Ozdogan et al., 2010; Salmon et al., 2015)

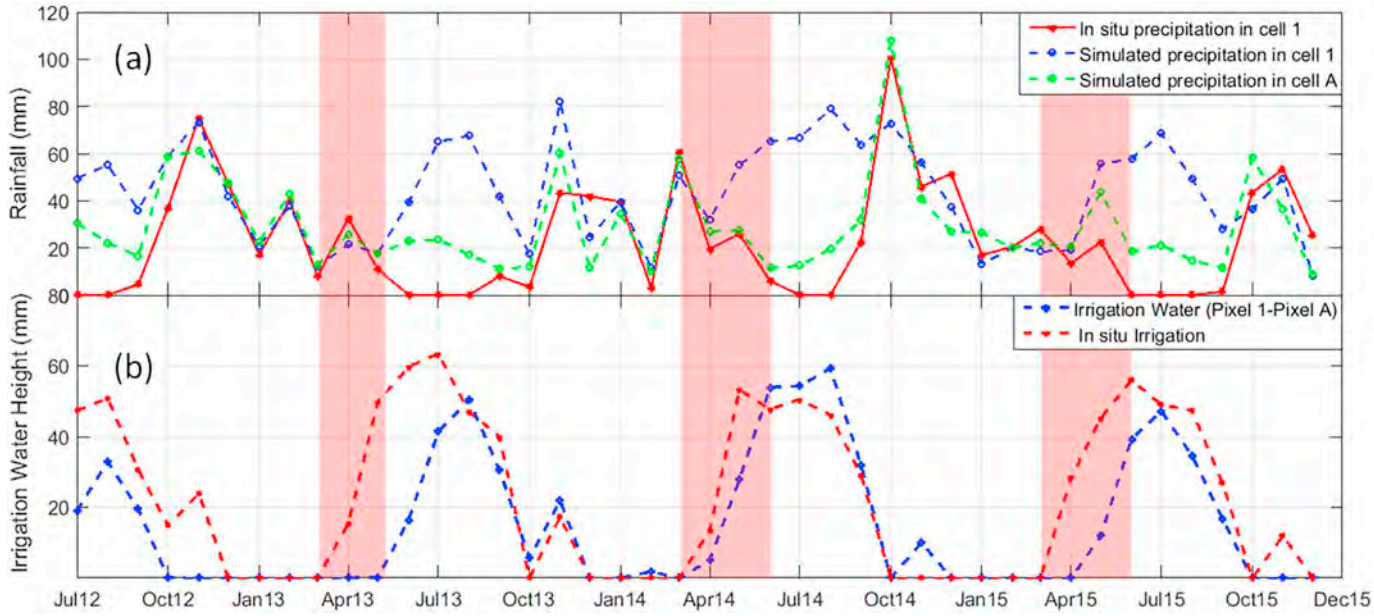

Fig. 11. a) The simulated precipitation in pixel (1) and A and in situ precipitation at pixel (1) and, b) comparison between bias-corrected irrigation estimates at pixel (1) and in situ irrigation at this pixel; highlighted period shows irrigation underestimation after the correction for bias.

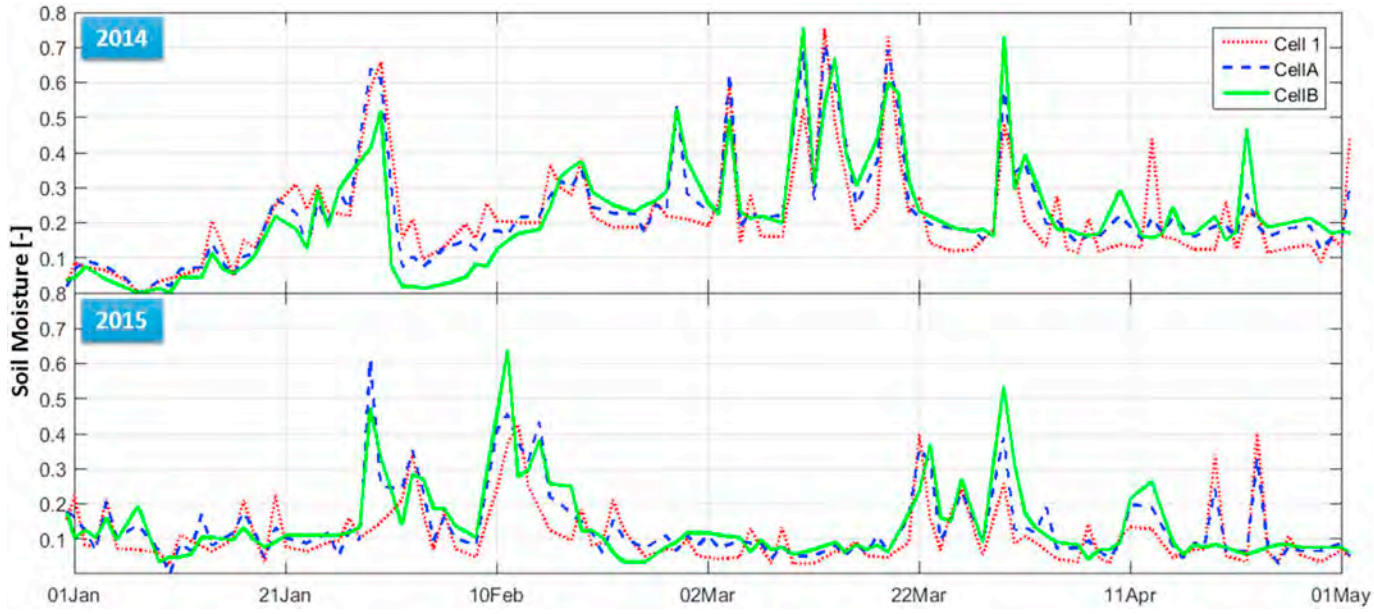

Fig. 12. Soil moisture dynamic in wet season of 2014 and 2015 in Pixel (1), (A) and (B); it seems that adjacent pixels follow the same soil moisture pattern, although; the vegetation density is different.

6. Conclusion

Irrigation agriculture is one of the biggest consumer of fresh water resources, hence it is crucial to have an accurate measurements of irrigation depth in cropland areas. Moreover, better measurements of irrigation can contribute to improved irrigation efficiency and management. In this study, the SM2RAIN algorithm is exploited to quantify the irrigation water in Miandoab plain (in Iran), mostly during the rainless periods. The results indicate that SM2RAIN model, applied to AMSR2-JAXA soil moisture product in the period 2012–2015, can capture temporal pattern in irrigation, but systematically overestimate the irrigation compare to the in situ data. This can be related to either not including ground water resources in the in situ irrigation data or the bias in the SM2RAIN-estimated irrigation. To remove the possible error, the difference between simulated irrigation at an irrigated and non-irrigated pixel (model bias) is calculated and the bias-corrected irrigation is compared with in situ irrigation data at the monthly time scale. The results shows that by correcting for the bias, the model is capable of quantifying irrigation water consistent with observed data with average $R = 0.86$ and RMSE = 12.89 (mm/month). The model is also sensitive to the accuracy of the input data and using the more reliable ETa and P data can boost the model performance by > 40% in terms of RMSE.

The spurious irrigation signal in the non-irrigation periods caused by either the noise in soil moisture or error on observed rainfall data can result in estimating negative irrigation. However, the results confirms that on average, the negative irrigation is less than a third of estimated positive irrigation. Due to coarse resolution of the MW satellite, irrigation is only detected where large area, compare to the

satellite footprint (e.g. > 500 km^2), are irrigated within a short period of time (e.g. several days), thereby creating strong SM signal. However, the SM irrigation signal can be still overshadowed by a rainfall event when they occur simultaneously. So it is expected that model better reproduce the irrigation signal in the regions with prolonged periods of low (or no) rainfall.

Using a linear approximation for estimation of ETa allows capturing the irrigation seasonality based on mainly one input (i.e. SM), however; it leads to underestimation of ETa and consequently irrigation. This limitation can be overcome by employing the recently-developed data-driven approach (based on SM data) that estimate ETa through parameterization of the loss functions. Thereby, there is a good potential for developing a stand-alone irrigation estimation method from microwave SM observation with a higher accuracy.

The quality of soil moisture retrieval is also important. Pixels should not containing urban areas, complex topography, marches and water bodies. The low spatial resolution of AMSR2 soil moisture product makes it impractical to capture the irrigation water of small irrigated area and higher resolution products (e.g., by Sentinel-1 or SMAP enhanced 9 km product) should be employed in future investigations.

Acknowledgements

The first author gratefully acknowledges support from the Iranian Ministry of Science, Research and Technology that makes this research possible. Luca Brocca acknowledges the support of European Space Agency through the project WACMOS-Irrigation (ESA EXPRO RFP/3-14680/16/I-NB). We also thank four anonymous reviewers and remote sensing of environment editorial team for the scrupulous attention to the details which help us to think outside the box. We believe that the paper has improved substantially thanks to their comments and feedb

Appendix A. Supplementary data

Supplementary data to this article can be found online at https://doi.org/10.1016/j.rse.2019.111226.

References

AghaKouchak, A., Norouzi, H., Madani, K., Mirchi, A., Azarderakhsh, M., Nazemi, A., Nasrollahi, N., Farahmand, A., Mehran, A., Hasanzadeh, E., 2015. Aral Sea syndrome desiccates Lake Urmia: call for action. J. Great Lakes Res. 41, 307–311. https://doi.org/10.1016/j.jglr.2014.12.007.

Akbar, R., Short Gianotti, D.J., McColl, K.A., Haghighi, E., Salvucci, G.D., Entekhabi, D., 2018. Estimation of landscape soil water losses from satellite observations of soil moisture. J. Hydrometeorol. 19, 871–889.

Alter, R.E., Im, E.-S., Eltahir, E.A.B., 2015. Rainfall consistently enhanced around the Gezira scheme in East Africa due to irrigation. Nat. Geosci. 8, 763–767. https://doi.org/10.1038/ngeo2514.

Ambika, A.K., Mishra, V., 2016. Remotely sensed high resolution irrigated area mapping in India for 2000 to 2015. Sci. Data 3, 160118.

Bagheri, M., Morid, S., Arshad, S., 2017. Application of remotely-sensed data to estimate a water budget for data-scarce endorheic basins: a case study of Lake Urmia basin, Iran. J. Indian Soc. Remote Sens. 45, 101–112.

Bastiaanssen, W.G.M., Cheema, M.J.M., Immerzeel, W.W., Miltenburg, I.J., Pelgrum, H., 2012. Surface energy balance and actual evapotranspiration of the transboundary Indus Basin estimated from satellite measurements and the ETLook model. Water Resour. Res. 48. https://doi.org/10.1029/2011WR010482.

Beck, H.E., Van Dijk, A.I.J.M., Levizzani, V., Schellekens, J., Miralles, D.G., Martens, B., De Roo, A., 2017. MSWEP: 3-hourly 0.25° global gridded precipitation (1979-2015) by merging gauge, satellite, and reanalysis data. Hydrol. Earth Syst. Sci. 21, 589–615. https://doi.org/10.5194/hess-21-589-2017.

Bindlish, R., Cosh, M.H., Jackson, T.J., Koike, T., Fujii, H., Chan, S.K., Asanuma, J., Berg, A., Bosch, D.D., Caldwell, T., Collins, C.H., McNairn, H., Martinez-Fernandez, J., Prueger, J., Rowlandson, T., Seyfried, M., Starks, P., Thibeault, M., Van Der Velde, R., Walker, J.P., Coopersmith, E.J., 2018. GCOM-W AMSR2 soil moisture product validation using core validation sites. IEEE J. Sel. Top. Appl. Earth Obs. Remote Sens. 11, 209–219. https://doi.org/10.1109/JSTARS.2017.2754293.

Breña-Naranjo, J.A., Kendall, A.D., Hyndman, D.W., 2014. Improved methods for satellite-based groundwater storage estimates: a decade of monitoring the high plains aquifer from space and ground observations. Geophys. Res. Lett. 41, 6167–6173.

Brocca, L., Moramarco, T., Melone, F., Wagner, W., 2013. A new method for rainfall estimation through soil moisture observations. Geophys. Res. Lett. 40, 853–858.

Brocca, L., Ciabatta, L., Massari, C., Moramarco, T., Hahn, S., Hasenauer, S., Kidd, R., Dorigo, W., Wagner, W., Levizzani, V., 2014. Soil as a natural rain gauge: estimating global rainfall from satellite soil moisture data. J. Geophys. Res. Atmos. 119, 5128–5141. https://doi.org/10.1002/2014JD021489.

Brocca, L., Massari, C., Ciabatta, L., Moramarco, T., Penna, D., Zuecco, G., Pianezzola, L., Borga, M., Matgen, P., Martínez-Fernández, J., 2015. Rainfall estimation from in situ soil moisture observations at several sites in Europe: an evaluation of the SM2RAIN algorithm. J. Hydrol. Hydromechanics 63, 201–209. https://doi.org/10.1515/johh-2015-0016.

Brocca, L., Pellarin, T., Crow, W.T., Ciabatta, L., Massari, C., Ryu, D., Su, C.H., Rüdiger, C., Kerr, Y., 2016. Rainfall estimation by inverting SMOS soil moisture estimates: a comparison of different methods over Australia. J. Geophys. Res. Atmos. 121, 12,062–12,079. https://doi.org/10.1002/2016JD025382.

Ciabatta, L., Marra, A.C., Panegrossi, G., Casella, D., Sanò, P., Dietrich, S., Massari, C., Brocca, L., 2017. Daily precipitation estimation through different microwave sensors: verification study over Italy. J. Hydrol. 545, 436–450. https://doi.org/10.1016/j.jhydrol.2016.12.057.

Döll, P., Siebert, S., 2002. Global modeling of irrigation water requirements. Water Resour. Res. 38, 8–10. https://doi.org/10.1029/2001WR000355.

Droogers, P., Immerzeel, W.W., Lorite, I.J., 2010. Estimating actual irrigation application by remotely sensed evapotranspiration observations. Agric. Water Manag. 97, 1351–1359.

Escorihuela, M.J., Quintana-Seguí, P., 2016. Comparison of remote sensing and simulated soil moisture datasets in Mediterranean landscapes. Remote Sens. Environ. 180, 99–114.

Forootan, E., Rietbroek, R., Kusche, J., Sharifi, M.A., Awange, J.L., Schmidt, M., Omondi, P., Famiglietti, J., 2014. Separation of large scale water storage patterns over Iran using GRACE, altimetry and hydrological data. Remote Sens. Environ. 140, 580–595. https://doi.org/10.1016/j.rse.2013.09.025.

Haddeland, I., Skaugen, T., Lettenmaier, D.P., 2007. Hydrologic effects of land and water management in North America and Asia: 1700–1992. Hydrol. Earth Syst. Sci. Discuss. 11, 1035–1045.

Hain, C.R., Crow, W.T., Anderson, M.C., Yilmaz, M.T., 2015. Diagnosing neglected soil moisture source–sink processes via a thermal infrared–based two-source energy balance model. J. Hydrometeorol. 16, 1070–1086. https://doi.org/10.1175/JHM-D-14-0017.1.

Hassanzadeh, E., Zarghami, M., Hassanzadeh, Y., 2012. Determining the main factors in declining the Urmia Lake level by using system dynamics modeling. Water Resour. Manag. 26, 129–145. https://doi.org/10.1007/s11269-011-9909-8.

Jackson, T.J., Schmugge, T.J., 1991. Vegetation effects on the microwave emission of soils. Remote Sens. Environ. 36, 203–212. https://doi.org/10.1016/0034-4257(91)90057-D.

Kalma, J.D., McVicar, T.R., McCabe, M.F., 2008. Estimating land surface evaporation: a review of methods using remotely sensed surface temperature data. Surv. Geophys. 29, 421–469. https://doi.org/10.1007/s10712-008-9037-z.

Kim, S., Liu, Y.Y., Johnson, F.M., Parinussa, R.M., Sharma, A., 2015. A global comparison of alternate AMSR2 soil moisture products: why do they differ? Remote Sens. Environ. 161, 43–62. https://doi.org/10.1016/j.rse.2015.02.002.

Koike, T., 2013. Description of the GCOM-W1 AMSR2 soil moisture algorithm. Descr. GCOM-W1 AMSR2 Lev. 1R Lev. 2, 1–8.

Koster, R.D., Brocca, L., Crow, W.T., Burgin, M.S., De Lannoy, G.J.M., 2016. Precipitation estimation using L-band and C-band soil moisture retrievals. Water Resour. Res. 52, 7213–7225.

Koster, R.D., Reichle, R.H., Mahanama, S.P.P., 2017. A data-driven approach for daily real-time estimates and forecasts of near-surface soil moisture. J. Hydrometeorol. 18, 837–843. https://doi.org/10.1175/JHM-D-16-0285.1.

Kumar, S.V., Peters-Lidard, C.D., Santanello, J.A., Reichle, R.H., Draper, C.S., Koster, R.D., Nearing, G., Jasinski, M.F., 2015. Evaluating the utility of satellite soil moisture retrievals over irrigated areas and the ability of land data assimilation methods to correct for unmodeled processes. Hydrol. Earth Syst. Sci. 19, 4463–4478. https://doi.org/10.5194/hess-19-4463-2015.

Lawston, P.M., Santanello, J.A., Kumar, S.V., 2017. Irrigation signals detected from SMAP soil moisture retrievals. Geophys. Res. Lett. 44, 11,860–11,867. https://doi.org/10.1002/2017GL075733.

Li, Z.-L., Tang, R., Wan, Z., Bi, Y., Zhou, C., Tang, B., Yan, G., Zhang, X., 2009. A review of current methodologies for regional evapotranspiration estimation from remotely sensed data. Sensors 9, 3801–3853. https://doi.org/10.3390/s90503801.

Mahab Ghods Consulting Engineering, C, 2010. Study and Executive Status of Zarrineh Rood Projects. (Tehran).

Malbéteau, Y., Merlin, O., Balsamo, G., Er-Raki, S., Khabba, S., Walker, J.P., Jarlan, L., 2018. Toward a surface soil moisture product at high spatiotemporal resolution: temporally interpolated, spatially disaggregated SMOS data. J. Hydrometeorol. 19, 183–200. https://doi.org/10.1175/JHM-D-16-0280.1.

Martens, B., Miralles, D.G., Lievens, H., van der Schalie, R., de Jeu, R.A.M., Fernández-Prieto, D., Beck, H.E., Dorigo, W.A., Verhoest, N.E.C.C., 2017. GLEAM v3: satellite-based land evaporation and root-zone soil moisture. Geosci. Model Dev. 10, 1903–1925. https://doi.org/10.5194/gmd-10-1903-2017.

McColl, K.A., Alemohammad, S.H., Akbar, R., Konings, A.G., Yueh, S., Entekhabi, D., 2017. The global distribution and dynamics of surface soil moisture. Nat. Geosci. 10, 100–104. https://doi.org/10.1038/ngeo2868.

Ozdogan, M., Gutman, G., 2008. A new methodology to map irrigated areas using multi-temporal MODIS and ancillary data: an application example in the continental US. Remote Sens. Environ. 112, 3520–3537.

Ozdogan, M., Yang, Y., Allez, G., Cervantes, C., 2010. Remote sensing of irrigated agriculture: opportunities and challenges. Remote Sens. 2, 2274–2304. https://doi.org/10.3390/rs2092274.

Peña-Arancibia, J.L., McVicar, T.R., Paydar, Z., Li, L., Guerschman, J.P., Donohue, R.J.,

Dutta, D., Podger, G.M., van Dijk, A.I.J.M., Chiew, F.H.S., 2014. Dynamic identification of summer cropping irrigated areas in a large basin experiencing extreme climatic variability. Remote Sens. Environ. 154, 139–152. https://doi.org/10.1016/j.rse.2014.08.016.

Peña-Arancibia, J.L., Mainuddin, M., Kirby, J.M., Chiew, F.H.S., McVicar, T.R., Vaze, J., 2016. Assessing irrigated agriculture's surface water and groundwater consumption by combining satellite remote sensing and hydrologic modelling. Sci. Total Environ. 542, 372–382. https://doi.org/10.1016/j.scitotenv.2015.10.086.

Pengra, B., 2012. The Drying of Iran's Lake Urmia and its Environmental Consequences. UNEP-GRID, Sioux Falls (UNEP Glob. Environ. Alert Serv).

Qiu, J., Gao, Q., Wang, S., Su, Z., 2016. Comparison of temporal trends from multiple soil moisture data sets and precipitation: the implication of irrigation on regional soil moisture trend. Int. J. Appl. Earth Obs. Geoinf. 48, 17–27. https://doi.org/10.1016/j.jag.2015.11.012.

Romaguera, M., Krol, M., Salama, M., Su, Z., Hoekstra, A., 2014. Application of a remote sensing method for estimating monthly blue water evapotranspiration in irrigated agriculture. Remote Sens. 6, 10033–10050. https://doi.org/10.3390/rs61010033.

Salmon, J.M., Friedl, M.A., Frolking, S., Wisser, D., Douglas, E.M., 2015. Global rain-fed, irrigated, and paddy croplands: a new high resolution map derived from remote sensing, crop inventories and climate data. Int. J. Appl. Earth Obs. Geoinf. 38, 321–334. https://doi.org/10.1016/j.jag.2015.01.014.

Singh, D., Gupta, P.K., Pradhan, R., Dubey, A.K., Singh, R.P., 2017. Discerning shifting irrigation practices from passive microwave radiometry over Punjab and Haryana. J. Water Clim. Chang. 8, 303–319. https://doi.org/10.2166/wcc.2016.122.

Su, C.H., Ryu, D., Western, A.W., Wagner, W., 2013. De-noising of passive and active microwave satellite soil moisture time series. Geophys. Res. Lett. 40, 3624–3630. https://doi.org/10.1002/grl.50695.

Thomson, K., 2003. World agriculture: towards 2015/2030: an FAO perspective. Land Use Policy 20, 375. https://doi.org/10.1016/S0264-8377(03)00047-4.

Tourian, M.J., Elmi, O., Chen, Q., Devaraju, B., Roohi, S., Sneeuw, N., 2015. A spaceborne multisensor approach to monitor the desiccation of Lake Urmia in Iran. Remote Sens. Environ. 156, 349–360.

Vörösmarty, C.J., Green, P., Salisbury, J., Lammers, R.B., 2000. Global water resources: vulnerability from climate change and population growth. Science 289, 284–288 (80-.).

Wagner, W., Brocca, L., Naeimi, V., Reichle, R., Draper, C., de Jeu, R., Ryu, D., Su, C.-H., Western, A., Calvet, J.-C., 2014. Clarifications on the “Comparison between SMOS, VUA, ASCAT, and ECMWF soil moisture products over four watersheds in US”. IEEE Trans. Geosci. Remote Sens. 52, 1901–1906.

Yekom Consulting Engineers, Y., 2016. The Practical Solution for Decreasing 40% of Agricultural Water Use in Zarinneh and Simineh Rood Basin (Part 6: The Current State and the Plan for Improving Irrigation Practice in Miandoab Region).

Youneszadeh Jalili, S., Daneshkar Arasteh, P., Kamali, M., 2017. Analytical study of land use changes (irrigated agriculture) in the watershed of Lake Urmia using Landsat imagery (in Persian). Sci. soil water 78.

Zaman, M.R., Morid, S., Delavar, M., 2016. Evaluating climate adaptation strategies on agricultural production in the Siminehrud catchment and inflow into Lake Urmia, Iran using SWAT within an OECD framework. Agric. Syst. 147, 98–110.